Defence Science Journal, Vol. 69, No. 4, July 2019, pp. 389-395, DOI : 10.14429/dsj.69.12135

Graceful Degradation: An Airborne Surveillance Radar Perspective

R. Rajesh*, Reena Sharma, and Suma Varughese
DRDO-Centre for Airborne Systems, Bengaluru - 560 037, India
**E-mail: rajesh@cabs.drdo.in*

ABSTRACT

Active electronically scanned antenna (AESA)-based radars imbibe the desirable feature of 'graceful degradation'. Such radars use miniaturised transmit-receive (TR) modules and a failure of few modules does not lead to failure of the mission. For example, in AESA-based ground MTI radar, failure of a few modules does not affect the array performance. In such a case, the static ground clutter is centred on zero frequency does not have a motion dependent Doppler spread. However, in airborne AESA radars, the ground clutter has an angle dependent Doppler frequency due to the platform motion and clutter leaking in through antenna side-lobes. Hence, the antenna side lobe levels dictate the side lobe clutter against which target detection is to be performed. The detection performance is governed by the signal to interference plus noise ratio (SINR). For Airborne surveillance radar the effect of random and systematic failures of TR modules and their effect on SINR is characterised. It is shown that single channel processing does not effectively provide the graceful degradation feature as the SINR loss due to failures is significant. However, the effect of systematic failure on SINR loss is less as compared to random failures. An effective scheme for feeding the array is also proposed.

Keywords: Graceful degradation; AESA; TR module; Random failure; SINR loss

NOMENCLATURE

M	Number of rows in antenna array
N	Number of columns in antenna array
q	No of bits in phase shifter & attenuator
dx	Inter-element spacing along length
dy	Inter-element spacing across breadth
B	Instantaneous bandwidth
R	Power output per TR module
h	Platform height
v	Platform velocity
f_0	Centre frequency
λ	Wavelength
L	Number of array panels
A	Maximum phase shifter attenuation
θ	Elevation angle
ϕ	Azimuth Angle

1. INTRODUCTION

Airborne surveillance radars are migrating to AESA due to advantages like inertia less beam scanning, beam agility and graceful degradation. The basic building block of AESA radar is miniaturised transmitter and receiver behind each antenna element and is popularly known as the transmit – receive (TR) module. This arrangement distributes the transmitters and receivers across array elements bringing in robustness against single point failures in the system. One of the prime advantages of this technology is that failure of a few modules does not degrade the performance of the radar leading to mission failure. Hence the mean time between critical failures (MTBCF) of such arrays is long and the radar is known to possess *'graceful degradation'* feature.

Ground-based long range AESA radars have typically more than a thousand TR modules. Failure of few modules does not significantly affect the detection performance as the gain of the array does not significantly reduce due to failure of few modules. The undesirable component ground clutter, entering through the side-lobes, falls around zero frequency. This zero frequency clutter can be effectively mitigated by adopting moving target indicator (MTI) or Doppler processing schemes. Hence the side lobe level increase or the distribution of the side-lobe energy in the antenna pattern is not a critical parameter for the ground-based MTI radars and such radars follow the 'graceful degradation' trend.

The situation is drastically different in airborne radars where the platform motion causes the clutter to inherit an angle dependent Doppler frequency. The main lobe clutter can be tracked and removed by clutter centroiding and MTI filtering technique. However, the side lobe clutter which spreads in frequency cannot be filtered out. The side-lobe clutter power depends on the antenna side-lobe levels and is dominated by inter-cardinal elevation side-lobes which illuminate the ground at near ranges. Hence, most long range airborne radars have ultra low-side-lobes which bring the side-lobe clutter energy below noise. The detection performance of such radars is affected by the antenna side lobe levels in addition to the main lobe. The characterisation of side lobes due to random

Received : 17 October 2017, Revised : 21 January 2019
Accepted : 19 February 2019, Online published : 15 July 2019

array failures is stochastic in nature and hence it is not clear if 'graceful degradation' still is applicable for airborne radars. This is due to the fact that increased side lobes due to the failure of TR modules can raise the clutter floor significantly resulting in considerable detection loss.

2. RELATED WORK

AESA radars are commonly used in long range airborne surveillance radars, providing high availability and performance. The distinguishing feature of an AESA is that it can have failed elements and still operate at high performance levels. The failure of TR modules is usually due to the failure of power amplifier, the low noise amplifier (LNA) or the control circuitry. The control circuitry typically controls multiple TR modules. The mean time between failures (MTBF) of TR modules for robust designs is discussed by Agrawal[1]. The characterisation of the TR module failures in terms of amplitude and phase errors for a large space-based array for anti-jam performance is characterised by Wang[2]. The directivity loss and the mean far side-lobe ratio are computed in terms of the error statistics. The work is extended to include manufacturing errors in Wang[3]. The effect of analysis of non-uniformity of array elements is also provided by Skolnik[4]. The degraded pattern is expressed as a function of the variances of the amplitude errors, phase errors and percentage of failed elements in Shahmiran[5]. Effect of module failures is also characterised for one dimensional phased array in Guodang[6] and is concluded that deterioration in gain is less than that of the side-lobes. Correction of antenna pattern for large monopulse-based arrays is discussed in Keizer[7]. Phase randomisation-based techniques to combat quantisation errors are given in Kamoda[8].

None of the above works throw light on the effect of array failures on inter-cardinal side-lobes that are critical for airborne radar. Most of the side-lobe clutter enters the radar through the inter-cardinal side-lobes that touch the near ranges. In this paper, the effect of array ageing effects is holistically characterised from increase in side-lobe clutter due to the array failures and its effect on the radar detection performance. The performance is characterised for random failures, systematic failures, and loss in calibration.

Simulation of ground clutter radar returns accounting the 3D antenna pattern, both in transmit and receive is an important part of this work. The clutter simulation is performed using techniques provided in Skolnik[9] and Ward[10].

3. AESA-BASED AIRBORNE RADAR MODEL

Consider airborne surveillance radar flying with velocity of v m/s at a height of h feet above the ground. The radar transmits electromagnetic waves with centre frequency f_0 and bandwidth B. The radar has to detect airborne targets against urban ground clutter. The radar has an AESA planar antenna array comprising of radiating elements arranged in a rectangular grid. The grid has M rows and N columns. Hence the total number of elements in the array is MN. The inter element spacing $dx = dy = \lambda/2$, where dx and dy are the inter element spacing along length and breadth respectively and λ is the wavelength. The radiating element has pattern of $\cos^{n1}\theta$ and $\cos^{n2}\theta$ in the azimuth and elevation directions respectively where n_1 and n_2 are chosen according to the type and dimension of the radiating elements and they control the active element beam width. The antenna array is divided into L panels for ease of fabrication and maintenance.

There is a TR module feeding each of the MN array elements. Each TR module can provide R watts of power. The TR module has 2^q phase and amplitude states, where q is the number of bits of phase shifter and attenuator. The TR module is packed into multi-modules with a common control circuitry and is called TRMM. Without loss of generality, each TRMM has M TR modules. The output of TR modules inside a TRMM are combined used a power combiner which is also assumed to be part of the TRMM. A TRMM can feed a column of the array and hence N TRMMs feed the whole array. The TR module in a single panel is powered by a power supply bank which is kept near the modules. Since, there are L panels, L such power supply banks are required. The power supply banks are assumed to have power modules inside. The AESA configuration is depicted in Fig. 1. The output of the TRMM is combined by a beam forming network to produce the array output channel and the monopulse channels. These channels are used for target detection and estimation of parameters like target location and velocity.

The array is assumed to be operating in the narrow band regime where the bandwidth is only a small percentage of the centre frequency. This allows for the approximation of time delays by phase shifts[11]. The antenna pattern is described in terms of the azimuth angle (ϕ) and elevation angle (θ). A steering vector-based formulation is adopted for antenna pattern computation. This formulation has the advantage that it can incorporate the array ageing effects in terms of vectors and matrices and makes the notation easier. Let $\otimes$ denote the Kronecker product of two matrices and $\odot$ denote the point by point or Hadamard product. Define

$$p_{a0} = 2\pi \frac{dx}{\lambda} \sin(\phi_0) \cos(\theta_0) \quad (1)$$

$$p_{b0} = 2\pi \frac{dy}{\lambda} \sin(\theta_0) \quad (2)$$

where (ϕ_0, θ_0) is the array look direction. The array is scanned to (ϕ_0, θ_0) by providing progressive phase shifts of $mp_{ao} + n\,p_{bo}$ to each of the elements of the array, where m varies from $[1:M]$ and n varies from $[1:N]$. Define column vectors

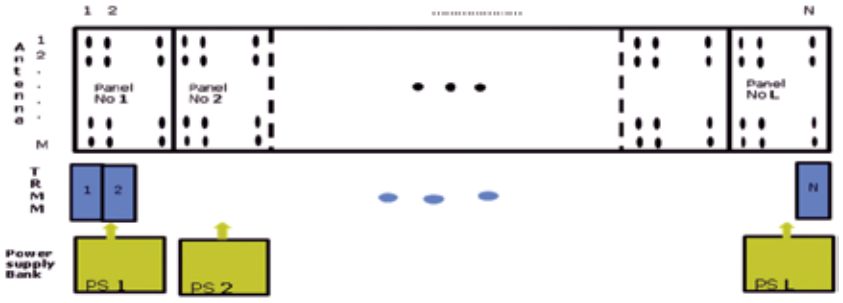

Figure 1. AESA antenna configuration.

$$X_0 = \begin{bmatrix} 1 & e^{-jp_{ao}} & e^{-j2p_{ao}} \ldots e^{-j(N-2)p_{ao}} & e^{-j(N-1)p_{ao}} \end{bmatrix}^T \quad (3)$$

and

$$Y_0 = \begin{bmatrix} 1 & e^{-jp_{bo}} & e^{-j2p_{bo}} \ldots e^{-j(M-2)p_{bo}} & e^{-j(M-1)p_{bo}} \end{bmatrix}^T \quad (4)$$

Then

$$Z_0 = X_0 \otimes Y_0 \quad (5)$$

denotes the MN dimensional steering vector that corresponds to the look direction. The response at any direction (ϕ, θ) can be found out by the defining

$$p_a = 2\pi \frac{dx}{\lambda} \sin(\phi) \cos(\theta) \quad (6)$$

$$p_b = 2\pi \frac{dy}{\lambda} \sin(\theta) \quad (7)$$

and defining of column vectors X and Y similar to (3) and (4) and computing $Z = X \otimes Y$.

The array factor is given by

$$AF(\phi, \theta) = Z^H Z_0 \quad (8)$$

where $(.)^H$ is the Hermitian transpose.

The incorporation of array weighting to reduce side lobes is done as follows. Let W_1 be the weighting along length of the array and W_2 be along the breadth. The combined MN dimensional weighting is

$$W = W_1 \otimes W_2 \quad (9)$$

The weighting is different for transmit and receive patterns. The weighting is usually uniform in transmit and Taylor or Chebyshev in receive.

The array factor with weighting is given by

$$AF(\phi,\theta) = Z^H \left(W \odot Z_0\right) \quad (10)$$

Let b_1 and b_2 represent the residual bit errors in amplitude and phase respectively. A q bit attenuator and phase shifter will provide a resolution of $r_p = 2\pi / 2^q$ radians of phase resolution and $r_a = A / 2^q$ dB of amplitude resolution, where A is the maximum attenuation in dB. Typically, $A = 32$. The mean phase error in radians is $E_p = b_1 r_p$ and mean amplitude error in dB is $E_a^{'} = b_2 r_p$. Both the amplitude and phase errors are assumed to be distributed uniformly. The amplitude error in the linear scale is given by Eqn. (11).

$$E_a = 10^{\frac{Ea'}{20}} \quad (11)$$

Let $\boldsymbol{U}$ be a random variable uniformly distributed in $[0,1]$. The phase error for each of the MN dimensional elements is of the form $P_e = e^{j\left(-E_p + 2E_p U\right)}$ and the amplitude error is $A_e = -E_a + 2E_a \boldsymbol{U}$. Let P and A be MN dimensional vectors having phase and amplitude errors with the distribution given above. Then the array factor is provided by

$$AF(\phi,\theta) = Z^H((W \odot Z_0) \odot P_e \odot A_e) \quad (12)$$

The AF is computed for each (ϕ, θ) and it gives the 3D array pattern. This is further multiplied by the element pattern $E(\phi, \theta)$ to obtain the overall antenna pattern.

$$P(\phi,\theta) = AF(\phi,\theta) \odot E(\phi,\theta) \quad (13)$$

The overall antenna pattern can be different for transmit and receive as the weighting functions chosen can be different.

3.1 Simulation Setup

For quantifying the various real world array effects, the following parameters described in Table 1 are considered for simulation.

Table 1. Simulation parameters

Parameter	Value
h	30000 feet
v	125 m/s
f_0	3 GHz
B	4MHz
R	100W
M	10
N	100
L	10
n_1	0.8
n_2	2

The effect of 0.5 bit of residual error in calibration is characterised by choosing suitable b_1 and b_2. This is used to represent the real world pattern of the AESA. The difference between this pattern and the ideal pattern is in the side lobe structure. The antenna pattern is uniform in transmit and has weighting in receive for side lobe control. The weights chosen in receive is Taylor with -35 dB side lobe, $\bar{n} = 5$ along the length and -25dB side lobe, $\bar{n} = 4$ along the breadth. These patterns are representative and the conclusions hold in general. Figure 1 shows the receive pattern with 0.5 bit of residual error in both amplitude and phase. The comparison of various parameters like average side lobe level, inter-cardinal average side lobe level, cardinal side lobe level in azimuth, and cardinal side lobe level in elevation is as tabulated in Table 2. The values are computed with averaging over Monte Carlo runs.

From the table it can be noticed that residual errors in calibration affects the inter-cardinal side lobes to a greater extent than the cardinal averages. However, the increase in side lobe levels is not considerable.

4. ARRAY AGEING EFFECTS AND ANTENNA PATTERN

TR modules-based on Gallium Arsenide (GaAs) microwave monolithic integrated circuits (MMIC) lead to the fielding of AESA-based radar systems. TR modules have the role of power amplification, signal reception, beam scanning, and beam shaping. These functionalities are achieved through a power amplifier, LNA with limiter, phase shifter, and attenuator respectively. The phase shifter, attenuator, and other controls can be often packed in a multi-functional chip often called core chip[12,13]. The component that is most prone to failure in a TR module is the power amplifier, mostly

Table 2. Comparison of antenna pattern parameters

Pattern	Average SLL (dB)	Inter-cardinal average SLL (dB)	Cardinal average SLL (Azimuth) (dB)	Cardinal average SLL (Elevation) (dB)
Ideal	-53	-64.8	-48.9	-32.3
Residual Error (0.5 bits)	-51	-61.4	-47.9	-32.2

due the self heating. Components like LNA and associate circuitry, control electronics, core chip, power converters can also fail.

From the configuration in Fig. 1, the following ageing effects can occur in the array

(i) Loss in calibration due to ageing of components
(ii) Failure of a few TR modules in a random fashion leading to random failures
(iii) Failure of one or few TRMM leading to column failures.

The first part of the paper characterises the effect of the above failures on the 3D antenna pattern of the array. The second part extends the study to how these antenna patterns affects the side lobe clutter levels and the subsequent detection loss. The relative severity of various errors will provide an assessment of the array feeding mechanism and the configuration of the TRMM and the PS.

4.1 Loss in Calibration

The loss in calibration occurs due to the ageing of components or a different operational condition, like change in temperature. The loss in calibration can be modelled by using the same model as residual bit errors. The values of b_1 and b_2 that denote the number of bits of amplitude and phase error are suitably adjusted to capture the effect of loss in calibration. The effect of loss in calibration is as provided in Fig. 3. The pattern parameter values are obtained using Monte Carlo runs.

It is found from Fig. 3 that the variation of pattern parameters due to calibration errors is almost linear. However, the calibration error has the maximum effect on the inter-cardinal side-lobe.

4.2 Random Failures

TR module failures occur usually due to the failure of the power amplifier or the LNA. The failure of power amplifier and LNA affects the transmit pattern and receive pattern respectively. The failure of any component in the common path (e.g., the core chip, power supply drive to each of the TR module) will affect both transmit and receive pattern. Radom failures are commonly defined by the percentage failure $(r\%)$. Then the total number of elements failed is

$$Q = ceil\left(\frac{rMN}{100}\right) \tag{14}$$

where ceil rounds the value to the nearest higher integer. An MN dimensional failure vector F_{rf} is constructed with 0s at Q positions and 1 s at the other positions. The Q positions are uniformly distributed integers in $[1, MN]$. The vector F may be different for transmit and receive depending of the type of components that have failed. The antenna pattern with random failure is as given by

$$AF_{rf}(\phi,\theta) = Z^H\left((W \odot Z_0) \odot P_e \odot A_e \odot F_{rf}\right) \tag{15}$$

$$P_{rf}(\phi,\theta) = AF_{rf}(\phi,\theta) \odot E(\phi,\theta) \tag{16}$$

A representative antenna pattern with 10 per cent random failures is as given in Fig. 4. A comparison between Fig. 2 and Fig. 4, shows the increase in inter-cardinal side lobes due to the random failure of the TR modules. The various pattern parameters for random errors are provided in Fig. 5. Also there is a gain loss of around 0.8 dB for 10 per cent random failure.

As evident from Figs. 4 and 5, the inter-cardinal side lobes show drastic increase due to random errors. Even 2 per cent random failure is enough to increase the inter-cardinal average by 10 dB. Also it can be noted that the cardinal average side lobes do not change drastically. Hence, any analysis-based on the cardinal average side lobe characteristics will fail to capture the effect of random TR module failures.

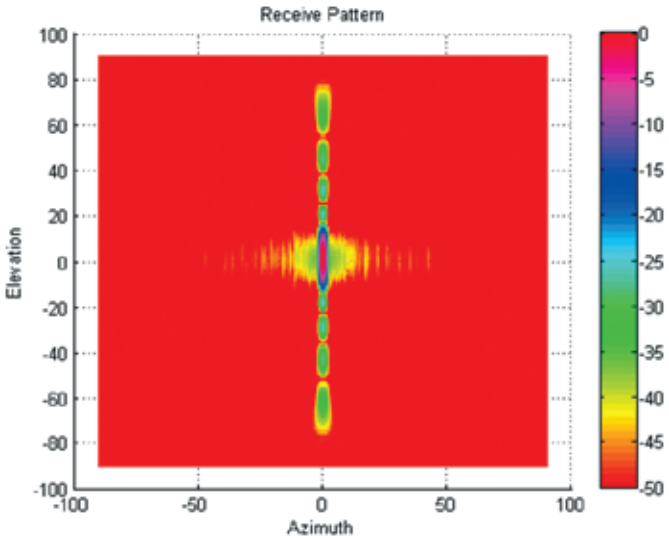

Figure 2. Receive pattern with 0.5 bit residual error.

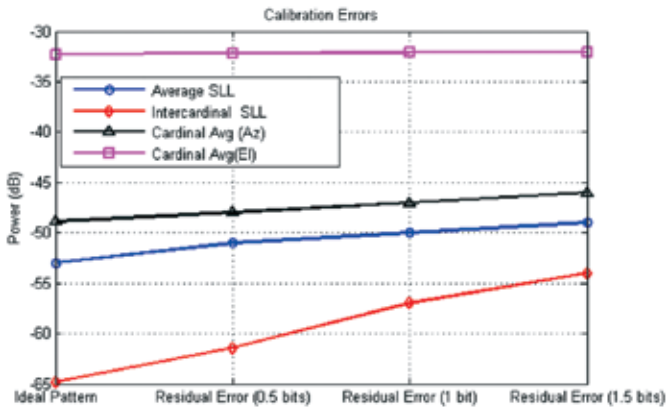

Figure 3. Pattern parameters with calibration error.

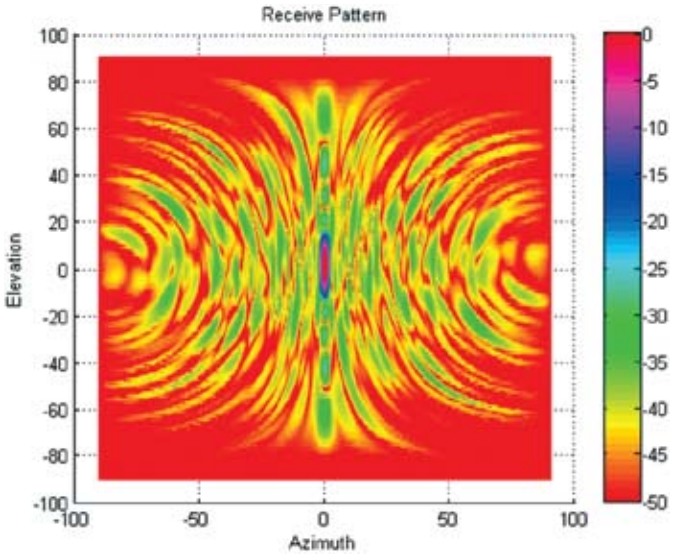

Figure 4. Antenna pattern with 10 per cent random errors.

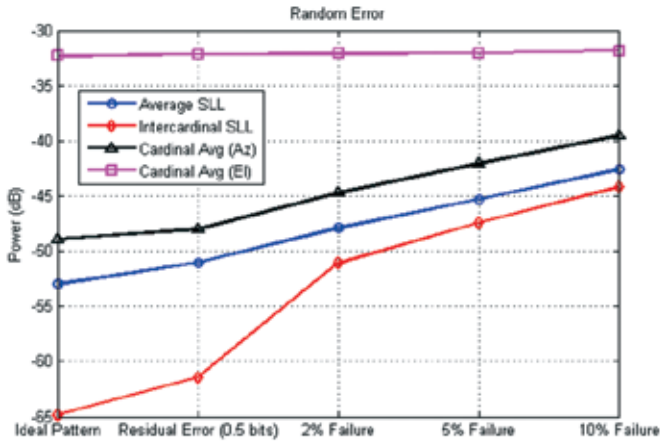

Figure 5. Pattern parameters with random error.

4.3 Column Failures

The column failure occurs due to failure of a TRMM. Multiple TRMM failures leads to multiple column failures. The *MN* dimensional failure vector F_{cf} can be obtained from an *M* dimensional vector F_1 of all ones and an *N* dimensional vector F_2 with all ones but for zeros in the position of columns which have failed. Hence,

$$F_{cf} = F_2 \otimes F_1 \quad (17)$$

and the corresponding patterns are found out by substituting F_{cf} instead of F_{rf} in Eqns. (15) and (16). The effect of antenna parameters on column failures is as given in Fig. 6.

As seen from Fig. 6, column errors effect the cardinal azimuth side lobes to a greater extent than the inter-cardinal side lobes. The comparison of the cardinal azimuth side lobes amongst various ageing effects is as given in Fig. 7. This also includes the power supply (PS) failure which can be modelled as multiple column failure.

It can be seen that the cardinal azimuth side lobe increase is least for the random errors and the most for power supply failures at the centre of the array. The side lobe increase due to column error is also significant. The interesting fact is that the increase in inter-cardinal side lobes follows a reverse trend

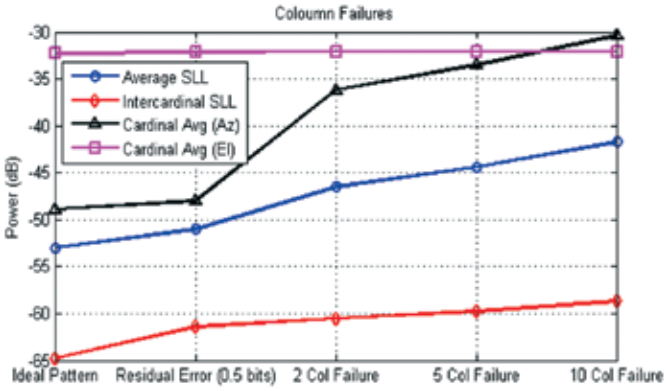

Figure 6. Pattern parameters with column error.

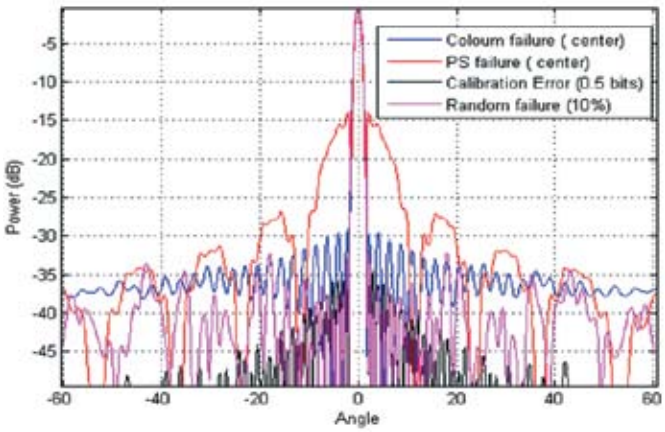

Figure 7. Comparison of average cardinal azimuth side lobes.

where the increase in side lobes is highest for the random errors and least for the power supply failures. This also brings in the need of a high fidelity clutter simulation to characterise the effect of degraded 3D antenna pattern due to failures.

5. AIRBORNE RADAR CLUTTER

The effect of the module failures in terms of the antenna parameters does not quantify its effect on radar detection or graceful degradation *per se*. Hence, it is important to quantify the effect of failures on radar clutter and the consequent SINR loss.

The ground clutter is assumed to have mean reflectivity, $\gamma = 0.15$, which corresponds to urban clutter. The radar operates at medium PRF of 10 KHz and 10 per cent duty cycle. The RD map and CNR are characterised for various failures using the antenna pattern given in Section 4. The rest of the parameters are as per Table 1.

The range-doppler (RD) map for the patterns in Fig. 2 and Fig. 4 are provided in Figs. 8 and 9, respectively. The effect of random failures is reflected as side lobe clutter in Fig. 9.

The RD map in Fig. 9 highlights the noise limited region, the side lobe clutter region and the main lobe clutter region. The side lobe clutter levels that arise due to the inter-cardinal side lobes are significant and this leads to detection loss in this region. The average clutter levels for the various cases in Fig. 7 are computed in Fig. 10 and it can be seen that the clutter level increase is maximum for random failures and relatively less for multiple column failures. Column feeding the array, as

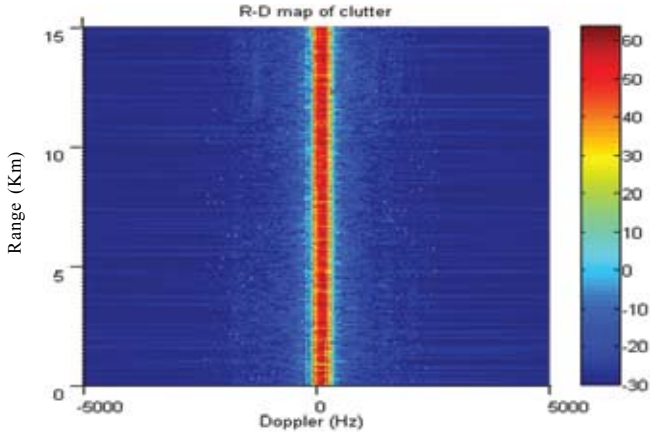

Figure 8. R-D map with 0.5 bit calibration error.

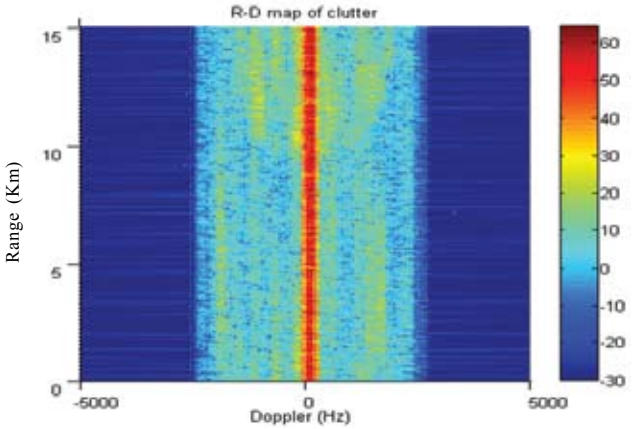

Figure 9. R-D map with 10 per cent random error.

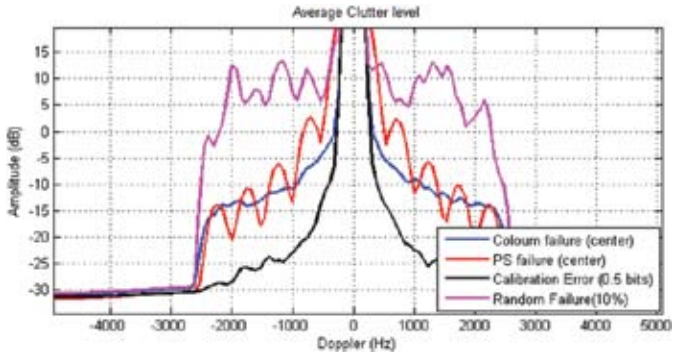

Figure 10. Average clutter levels.

proposed in the model, is efficient.

The average side-lobe clutter level is a direct indicator of the SINR loss given by

$$SINR_{Loss} = \sigma_n^2 + \sigma_c^2 \quad (18)$$

where σ_c^2 and σ_n^2 are clutter and noise variances respectively. The SINR loss is dominated by the inter-cardinal side lobes and hence maximum for random failures. The SINR loss can be directly translated to range loss via the radar equation.

6. CONCLUSIONS

The paper considered the generic problem of graceful degradation in airborne AESA radar used for long range surveillance. It is established that the inter-cardinal side lobe levels play a major role in determining side lobe clutter level. Also, the inter-cardinal side lobes are most sensitive to random failures than systematic failures. Hence, random feeding the array does not improve resilience to module failures. It can be concluded that the term 'graceful degradation' is conditional in airborne radars using conventional single channel processing. The 'graceful degradation' is valid only when the side-lobe clutter power with failures is comparable to noise level.

REFERENCES

1. Agrawal, A.K. & Holzmann, E.K. Active phased array design for high reliability. *IEEE Trans. Aerospace Electron. Sys.,* 1999, **35**(4), 1204-1211. doi:10.1109/7.805438
2. Wang, H.S.C. Performance of phased arrays under error condition. *IEEE Aerospace conference Digest*, USA, 1989, 1-25. doi: 10.1109/AERO.1989.82429
3. Wang, H.S.C. Performance of phased array antennas with mechanical errors. *IEEE Trans Aerospace Electron. Sys.*, 1992, **28**(2), 535-545. doi: 10.1109/7.144579
4. Skolnik, M.I. Non uniform array. *Antenna Theory,* 1969, R E Collin and F J Zuker (Eds), Mc Graw Hill Co, NY, Ch6.
5. Shahmirian, V. & Dayoush, A.S. Pattern degradation due to random errors in active phased array antenna. IEEE Antenna and Propagation Society International symposium, USA, 1989, 396-399. doi: 10.1109/APS.1989.134703
6. Guodang, H.; Mingwei, S. & Biao, D. Effect of sub-system failures on the performance of one dimensional phased array antenna. *IEEE ICMMT*, Shenzhen, China, 2012, 1-4. doi: 10.1109/ICMMT.2012.6230204
7. Keizer, P.M.N.W. Element failure correction for a large monopulse phased array antenna with active amplitude weighting. *IEEE Trans. Antenna Propag.*, 2007, **55**(8), 2211-2218. doi: 10.1109/TAP.2007.902008
8. Kamoda, H.; Tsumochi, J. & Suginoshita, F. Reduction in quantization lobes due to digital phase shifters for phased array radars. *Asia-Pacific Microwave Conference Proceedings (APMC),* Melbourne, 2011, pp. 1618-1621.
9. Skolnik, M.I. Introduction to radar systems (3rd ed.), Tata Mc Graw Hill, 2001.
10. J Ward, J. Space time adaptive processing for airborne radar. Technical report 1015, Lincon Laboratory, MIT, 1994.
11. Brown, A.D. Electronically scanned arrays- Matlab modelling and simulation. CRC, Taylor and Francis group, LLC, 2012.
12. Bentini, A.; Ciccognani, W.; Palamba, M.; Palombini, D. & Limiti, E. High density mixed signal RF front end electronics for TR modules. IEEE ESTEL, Rome, 2012, 713-718. doi: 10.1109/ESTEL.2012.6400127

13. Limiti, E.; Colangeli, S.; Bentini, A.; Ciccogani, W. Robust GaN MMIC chipset for TR module front end Integration. *Int. J. Microwave Opt. Technol.*, 2104, **9**(1), 6-12.

CONTRIBUTORS

Dr R. Rajesh, Scientist 'E', received his BTech in ECE from National Institute of Technology, Calicut, India in 2002 and PhD from Electrical Communication Engineering department, Indian Institute of Science, Bangalore, India in 2009. Since December 2002, he is working as a Scientist with Centre for Airborne Systems, DRDO, Bangalore, India. His areas of interest include Information Theory, Wireless Communication, Radar Systems and System Engineering. He is a recipient of Laboratory Scientist of the year award in 2006, DRDO Young Scientist award in 2008 and Technology group award in 2013 and 2018.
His contribution in this paper includes conceptualisation of the problem, mathematical formulation, analysis, simulation and preparation of the manuscript.

Dr Reena Sharma, Scientist 'G', received her MTech in radar and communication from IIT Delhi and PhD in Microwave Engineering from Indian Institute of Science in 1997. She was a post doctoral fellow at Helsinki University of Technology (HUT), Finland during 1999-2000. Since 2000 she is working with Centre for Airborne Systems, DRDO, Bangalore, where she is heading airborne system projects. Her areas of interest include Electromagnetics, Chiral Materials, System Simulation for airborne surveillance and System Engineering. She is recipient of Laboratory Scientist of the year award for year 2011 and Technology group award in 2013.
Her contributions in this paper include the overall architecture, guidance in the preparation of manuscript and in revision of the paper.

Ms Suma Varughese, Scientist 'H', received her MSc (Comp. Sci.) in 1988 and MS (Engg) on Antenna measurement techniques from Institute of Science, Bangalore. She joined LRDE, DRDO in 1989. She moved to CABS, DRDO, Bangalore to join a prestigious airborne programme in 2004. She currently is an outstanding scientist at CABS heading various airborne system projects. Her areas of interest include active array antennas, antenna measurement techniques, multi-sensor data fusion and system engineering. She is a recipient of IETE J C Bose gold medal for best paper in 1993, NRDC national award for PNFM software in 1995, IETE NM Saha best paper award in 2013 and DRDO Agni award in 2013.
Her contributions in this paper include the overall architecture, guidance in the preparation of manuscript and in revision of the paper.